





Development of a Planar Haptic Robot With Minimized Impedance

Keonyoung Oh , William Z. Rymer , Ilaria Plenzio , Ferdinando A. Mussa-Ivaldi, Seunghan Park, and Junho Choi 

Abstract—Several studies have reported that stroke survivors displayed improved voluntary planar movements when forces supporting the upper limb increased, and when impeding forces decreased. Earlier haptic devices interacting with the human upper limb were potentially impacted by undesired residual friction force and device inertia. To explore natural, undisturbed voluntary motor control in stroke survivors, we describe the development of a Decoupled-Operational space Robot for wide Impedance Switching (DORIS) with minimized mechanical impedances. This design is based on a novel decoupling mechanism separating the end effector from a manipulator. While the user manipulates the end effector freely inside the workspace of the decoupling mechanism, to which a manipulator of the robot is attached, the robot detects such change in position using a lightweight linkage system. The manipulator of the robot then follows such movements of the end effector swiftly. Consequently, the user can explore the extended workspace, which can be as large as the manipulator's workspace. Since the end effector is mechanically decoupled from the manipulators and actuators, the user can remain unaffected by the mechanical impedances of the manipulator. Mechanical impedances perceived by the user and bandwidth of the control system were estimated. The developed robot was capable of detecting larger maximum acceleration and larger jerk of the reaching movement in chronic stroke survivors with hemiparesis. We propose that this device can be utilized for evaluating voluntary motor control of the upper limb while minimizing the impact of robot inertia and friction forces on limb behavior.

Index Terms—User workspace, haptic robot, neurological disorder, upper limb, impedance.

Manuscript received November 25, 2019; revised June 4, 2020 and August 12, 2020; accepted November 5, 2020. Date of publication November 18, 2020; date of current version April 21, 2021. This work was supported by the under Grant 90RES5013 from the U.S. Department of Health and Human Services, Administration on Community Living, National Institute on Disability, Independent Living and Rehabilitation Research, Institutional program (project no. 2E30090) of Korea Institute of Science and Technology (KIST), NSF under Grant 1632259, and the Falk Foundation. (Corresponding author: Junho Choi.)

Keonyoung Oh, William Z. Rymer, and Ferdinando A. Mussa-Ivaldi are with the Shirley Ryan AbilityLab, and also with the Department of Physical Medicine and Rehabilitation, Feinberg School of Medicine, Northwestern University.

Ilaria Plenzio is with the Dipartimento di Informatica, Bioingegneria, Robotica e Ingegneria dei Sistemi (DIBRIS), University of Genova.

Seunghan Park is with the Center for Bionics, Korea Institute of Science and Technology (KIST).

Junho Choi is with the Center for Bionics, Korea Institute of Science and Technology (KIST), Seoul 02792, Korea (e-mail: junhochoi@kist.re.kr).

Digital Object Identifier 10.1109/TBME.2020.3038896

I. INTRODUCTION

A. Impedance of a Haptic Robot

SEVERAL studies have reported that stroke survivors showed improvement in voluntary motor control when their upper limbs are supported against gravity, and when other resisting forces against movements were sharply reduced [1]. To illustrate, in an earlier study from our own group, we provided chronic hemiparetic stroke survivors with external forces supporting the weight of the impaired upper limb against gravity using a low friction air-bearing. In the presence of such supporting forces, coupled with low friction forces, stroke survivors showed larger planar joint excursions, longer reaching distance, larger maximum velocities, more straight movement trajectories, and smoother velocity profiles of the affected limb. Conversely, additional mechanical impedances in the form of added inertia, stiffness, and viscosity induced changes in activation levels in upper limb muscles for target reaching in chronic stroke survivors [2]. These findings imply that additional loads on upper limb muscles should ideally be minimized if we wish to study undisturbed limb motion in stroke survivors. Our objective here then is to describe the design and initial testing of a haptic device that imposes minimal additional loads on the upper limb.

For assessing voluntary motor control accurately in human subjects who are receiving supporting forces against gravity, undesired impedances imposed by the supporting device should not disturb the user's natural movements. It follows that these impedances need to be kept as small as possible [3], [4]. For example, when an existing haptic device's impedances were compared to those of the related human joints, the device showed relatively larger impedances [3]. During a human reaching task, such additional impedance can induce different muscular activities in the upper limb muscles in stroke survivors as compared to those activities with other types of impedances [2]. In addition, an essential measure, which indicates smoothness of the arm movement, is the jerk [5] or the number of sub-movements [6]. Since the jerk can be strongly affected by the additional inertia of the robot, it is important to develop a haptic robot with minimized impedances to assess motor control, without any undesired disturbances or resisting forces.

A number of robotic devices have been developed to assess or to train the voluntary control of the upper limb with a greater range of motion. The Bi-Manu Track was developed to train the user's forearm and wrist [7]. For the bimanual movements, the Mirror Image Motion Enabler (MIME) was introduced so

the intact side of the upper limb can assist movements of the affected side of the upper limb [8]. The MIT MANUS [9], [10], InMotion Arm [11], and InMotion Wrist [12] were introduced for upper limb training in a 2D plane using the impedance control scheme. The Armeo Spring [13], Armin [14], BURT Robotic Arm [15], and HapticMaster [16], [17] enables users to interact with perturbations or virtual objects. These devices, however, routinely have non-negligible impedances associated with dynamic inertia of components, friction forces, and performance limits of the control system. For example, with the admittance control paradigm used in the HapticMaster and another programmable haptic robot [18], the end effector has to have a theoretical mass of at least 2 kg [16] and 1.7 kg [18], respectively, which is quite significant when compared to the mass of the upper limb. Since the admittance control paradigm measures contact forces exerted by a user and then generates resultant movements based on a predetermined theoretical mass of the end effector [19], a minimum non-zero mass is required to avoid a nearly infinite acceleration, which may result from a ratio of the non-zero contact force to the zero inertia.

To minimize additional impedances induced by the inertial resisting force, haptic robots characterized by high back-drivability have also been developed. To reduce the inertia imposed by the long, heavy linkage mechanisms, some haptic devices utilized thin, lightweight linkage systems or cable-driven systems to transmit actuating torques [3], [20], [21]. The inertia of one such device, the MIT MANUS [10], of a timing belt-driven robot, the vBOT [22], and also of a cable-driven haptic robot, CBM-Motus [23] were estimated to be 0.67 kg, 0.42-0.71 kg, and 2.026 kg, respectively. In addition, to minimize the effective inertia of the robotics, a feedforward controller was utilized to compensate the influence of the dynamic impedance of the robot, which includes joint friction, segment mass, and moment of inertia. These dynamic parameters were identified first and were compensated using the inverse dynamics algorithm and the feedforward impedance controller [24], [25]. To improve transparency of the haptic robot, impedances of the human hand were also identified to minimize the effects of force feedback between the user and robot [26].

Recently, some studies have developed the iterative or neural control strategies to facilitate effective, smooth human-robot interaction. The activation level and joint coordination of the upper limb muscles were first estimated. To realize sophisticated human-robot interaction as the user intended, the impedance of the end effector of the robot was then matched to those estimated impedance values [27], or control input was modulated online by adapting the feedforward force in the tracking task with the upper limb [28], [29].

In addition, a novel tracking control paradigm was introduced to allow the end effector to be unaffected by the robot's inertia by decoupling the end effector from its actuators [30], [31] and by extending a small workspace of the user [32] to a larger workspace of the actuators. The relatively small robotic end effector was introduced, which was passively attached to the large system, including actuators. Thus, the end effector could have a small range of undisturbed movements [30], [31]. When the user manipulates the end effector, and before the end effector

hits the boundary of the workspace, the workspace itself is also moving to follow the user's movement. Consequently, the size of the user's workspace can be extended to reach that of the actuators without increasing the impedance. This control strategy has been used to develop earlier manipulators [23], and we also adopted this control paradigm to develop a haptic robot with the relatively smaller impedances of the end effector than exhibited by other haptic robots.

B. Switchable Impedance of the Robot

Another benefit offered by haptic robots is providing the user with highly motivating interactive training. The various types of loads can be implemented by regulating impedances of the end effector. This type of robotic interface may be valuable as neurologic therapy and can make training situations more interesting, more diverse, and help a user focus more on the therapy [33].

To minimize additional impedances of the end effector while assessing motor control of the upper limb, we have developed a planar haptic robot, called Decoupled-Operational space Robot for wide Impedance Switching (DORIS). The unique control paradigm of the developed robot allows a user to be largely unaffected by external impedances of the robot. The impedances of the new robot and its control performance were quantified using sinusoidal excitation and step-input tests. Kinematics of the target reaching movements were then compared in chronic stroke survivors with hemiparesis between DORIS and another programmable robot, the HapticMaster. In addition, we implemented a switchable impedance to simulate a virtual wall using the brake system with an force/torque (FT) sensor.

II. METHODS

A. Design of DORIS

To guarantee that a user can remain largely unaffected by the impedances of the robot while manipulating the end effector, DORIS was designed around a unique mechanism incorporating a decoupled and extended user workspace. The end effector is passively connected to the decoupling mechanism through a pair of five-bar linkage system (four links and one frame) and low-friction bearings so that the end effector (with a handle attachment) can glide freely within the user workspace on the decoupling mechanism as the user intends (Fig. 1). The decoupling mechanism can detect such user's kinematic information from the end effector and then catches up with the end effector by minimizing the relative distance between the end effector and the center of the decoupling mechanism using three actuators connected to the translation links and rotation links (Fig. 2). Additional impedances imposed on the end effector are induced from the inertia of the end effector. Note that due to the decoupling mechanism, any impedances associated with the actuators and of the larger manipulator cannot be transmitted to the user who is grasping the handle attached to the end effector (Fig. 1). More detailed specifications of DORIS were in Table I.

The manipulator of DORIS has two different sets of linkage systems, which are separately responsible for the translational

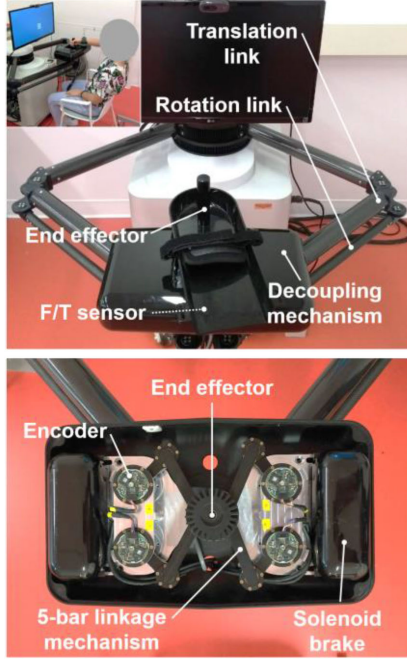


Fig. 1. (Top) Design of DORIS with the decoupled user workspace. The end effector (handle) can be moved freely within the decoupling mechanism, which is disjuncted from all the translation links, rotation links, and actuators. The inset figure represents a user manipulating the end effector of DORIS. (Bottom) Design of the decoupling mechanism. Four encoders at each corner are utilized for calculation of the position and angle of the end effector. When the brakes are engaged, the movement of the end effector is no longer allowed. Note that a handle is removed in the top figure to make the structure more clearly visible.

TABLE I
SPECIFICATIONS OF DORIS. ALL ARE MEASURED VALUES

Item	Value	Note
Max angular velocity of actuator (deg/s)	358	
Max angular acceleration of actuator (deg/s ²)	112	
Nominal force of decoupling mechanism (N)	375	At the farthest point from the base
Max speed of decoupling mechanism (m/s)	1.7	
Max acceleration of decoupling mechanism (m/s ²)	3.4	
Size of manipulator workspace (m ²)	0.5 · 0.5	
Size of user workspace (m ²)	0.065 · 0.065	
Max brake force (N)	36	
Position resolution (m)	1 · 10 ⁻⁶	
Force sensitivity (N)	1/16	
Max measurable force (N)	580 (x, y), 1160 (z)	

and rotational movement of the decoupling mechanism. The 2-dimensional (2-D) translation and 1-dimensional (1-D) rotation of the end effector could be immediately followed by the decoupling mechanism by controlling the translation and rotation links, respectively (Fig. 2). Four absolute encoders with

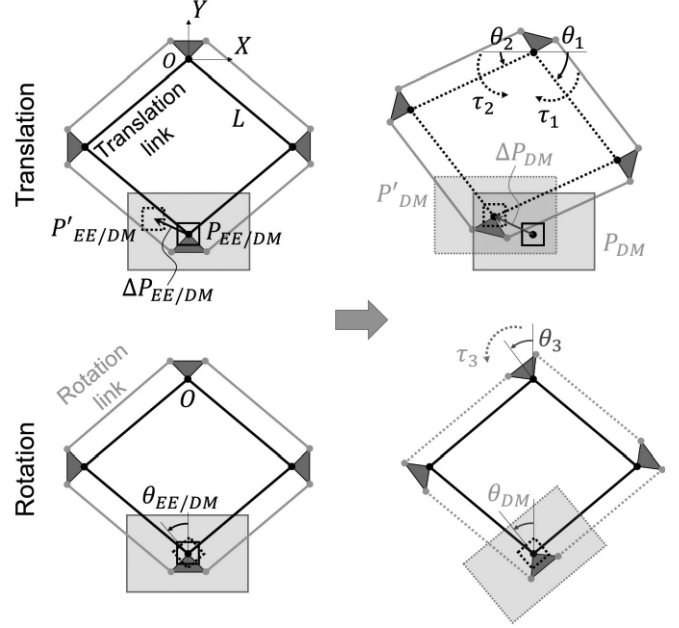


Fig. 2. DORIS can follow both a 2-D translational (up) and 1-D rotational (down) movement of a user. The decoupling mechanism detects the change in position of the end effector (from solid black square to dotted black square, $\Delta P_{EE/DM}$) and then tries to match the position of the center of decoupling mechanism (gray rectangular) with the new position of the end effector by controlling angles (θ_1 and θ_2) of the translation links (from solid to dashed black lines) by two separated actuators (τ_1 and τ_2). The rotation of the end effector (θ_{EE}) is also measured and the rotation link is then controlled (θ_3) (from solid to dashed gray lines) by an actuator (τ_3) to move the decoupling mechanism (θ_{DM}).

a resolution of 18 bits (EBI1135, Heidenhain, Traunreut, Germany) on the decoupling mechanism (Fig. 3) detect the change in position of the end effector ($\Delta P_{EE/DM}$ in Fig. 2) referenced to the center of the decoupling mechanism (P_{DM} in Fig. 2). For the translation of the end effector, either side of the translation link (θ_1 and θ_2 in Fig. 2) is then actuated by an identical motor (K127150, Parker Hannifin, Mayfield Heights, OH, US) to minimize the relative distance between the end effector and the center of the decoupling mechanism ($\Delta P_{EE/DM}$). The position (x_{DM}, y_{DM}) of the decoupling mechanism, which is denoted by P_{DM} , is given as follows.

$$\begin{aligned} x_{DM} &= L(\cos \theta_1 - \cos \theta_2), \\ y_{DM} &= L(\sin \theta_1 + \sin \theta_2), \end{aligned} \quad (1)$$

where L is the length of each segment of the manipulator.

For the relative rotation of the end effector ($\theta_{EE/DM}$), the third actuator controls the rotation of the decoupling mechanism (θ_{DM}) via the rotation link system (Fig. 2). The triangle-shaped piece near P_{DM} is attached to the decoupling mechanism, so it can transmit the rotational movement of the third actuator (θ_3) to the decoupling mechanism (θ_{DM}). Note that the triangle-shaped piece is a right-angle isosceles triangle so each link of the translational links and the rotational links and two adjacent triangular-shaped pieces form a parallelogram. The parallelograms preserve the orientation of the decoupling mechanism regardless of the translational movement of the manipulator

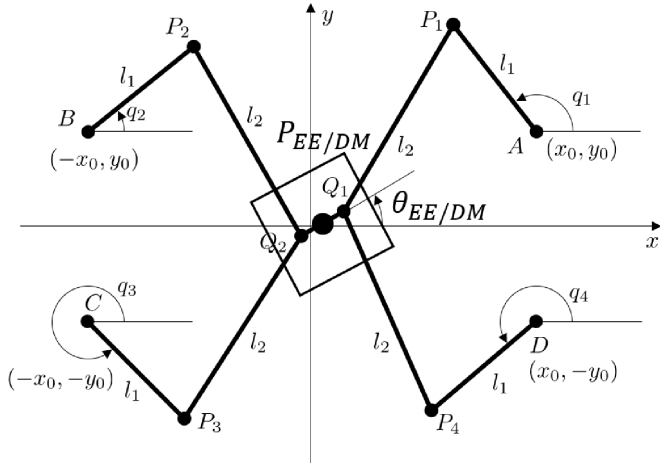


Fig. 3. Schematic of the five-bar linkage mechanism inside of the decoupling mechanism. The relative position ($P_{EE/DM}$) and relative rotation angle ($\theta_{EE/DM}$) of the end effector (solid black square) referenced to the decoupling mechanism can be obtained by using four measured angles ($q_1, q_2, q_3,$ and q_4) from absolute encoders. An origin point of the coordinate system coincides with the center point of the decoupling mechanism, P_{DM} in Fig. 2.

(Fig. 2). All the translational and rotational links are made of lightweight carbon fiber tubes and are connected to each other via passive revolute joints with low-friction bearings to reduce inertia and friction forces, respectively.

The end effector (or a handle attachment) is supported by a pair of identical five-bar linkage systems within the decoupling mechanism. Each linkage system connects two absolute encoders and the end effector, so the measured angles of each link are used to calculate the current position and rotation angle of the end effector (Fig. 3). The positions of revolute joints connecting two adjacent links are given as follows.

$$\begin{aligned} P_1 &= \begin{bmatrix} P_{1x} \\ P_{1y} \end{bmatrix} = \begin{bmatrix} l_1 \cos q_1 \\ l_1 \sin q_1 \end{bmatrix} + A, \\ P_2 &= \begin{bmatrix} P_{2x} \\ P_{2y} \end{bmatrix} = \begin{bmatrix} l_1 \cos q_2 \\ l_1 \sin q_2 \end{bmatrix} + B, \\ P_3 &= \begin{bmatrix} P_{3x} \\ P_{3y} \end{bmatrix} = \begin{bmatrix} l_1 \cos q_3 \\ l_1 \sin q_3 \end{bmatrix} + C, \\ P_4 &= \begin{bmatrix} P_{4x} \\ P_{4y} \end{bmatrix} = \begin{bmatrix} l_1 \cos q_4 \\ l_1 \sin q_4 \end{bmatrix} + D, \end{aligned} \quad (2)$$

where A , B , C , and D are the positions of the encoders (or end-points of each five-bar linkage system) and $q_1, q_2, q_3,$ and q_4 are the measured angles of the connected links (Fig. 3). Each five-bar linkage system is connected to the end effector at $Q_1 (x_1, y_1)$ and $Q_2 (x_2, y_2)$ via revolute joints.

Then, since the lengths of links are identical,

$$\begin{aligned} (x_1 - P_{1x})^2 + (y_1 - P_{1y})^2 &= l_2^2, \\ (x_1 - P_{4x})^2 + (y_1 - P_{4y})^2 &= l_2^2. \end{aligned} \quad (3)$$

Therefore,

$$y_1 = \alpha x_1 + \beta, \quad (4)$$

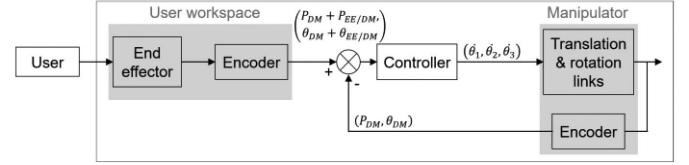


Fig. 4. A control block diagram of DORIS. Absolute encoders detect the user's translational and rotational movements and the control system tries to minimize relative movements ($P_{EE/DM}$ and $\theta_{EE/DM}$) of the end effector from the center of the decoupling mechanism (P_{DM} and θ_{DM}). In proportion to those relative movements, the velocity commands are sent to actuators to control the translation ($\dot{\theta}_1$ and $\dot{\theta}_2$) and rotation ($\dot{\theta}_3$) links.

where

$$\begin{aligned} \alpha &= \frac{P_{4x} - P_{1x}}{P_{1y} - P_{4y}}, \\ \beta &= \frac{P_{1x}^2 + P_{1y}^2 - P_{4x}^2 - P_{4y}^2}{2(P_{1y} - P_{4y})}. \end{aligned} \quad (5)$$

Then,

$$(1 + \alpha^2)x_1^2 + (-2P_{1x} + 2\alpha(\beta - P_{1y}))x_1 + P_{1x}^2 + (\beta - P_{1y})^2 - l_2^2 = 0. \quad (6)$$

Solving the equation yields the position of Q_1 . Similarly, the position of Q_2 is obtained. Then, the position and rotation angle of the end effector are given as

$$\begin{aligned} P_{EE/DM} &= \frac{(Q_1 + Q_2)}{2}, \\ \theta_{EE/DM} &= \tan^{-1} \frac{y_1 - y_2}{x_1 - x_2}, \end{aligned} \quad (7)$$

and used for the desired position and angle of the decoupling mechanism in the control system.

The calculated position ($P_{DM} + P_{EE/DM}$) and rotation angle ($\theta_{DM} + \theta_{EE/DM}$) of the end effector with respect to the origin point O (Fig. 2) are each specified as the desired position and rotation angle for the decoupling mechanism, so the control system then tries to minimize relative deviations (or feedback errors) of the end effector ($P_{EE/DM}$ and $\theta_{EE/DM}$) from the center of decoupling mechanism to track the user's movement (Figs. 2 and 4). The velocity commands, which are set in proportion to the feedback errors in the position and rotation angle, are sent to two actuators ($\dot{\theta}_1$ and $\dot{\theta}_2$) for the translation and to the third actuator ($\dot{\theta}_3$) for the rotation (Fig. 4). The feedback control system operates at 1 kHz.

B. Switchable Impedance Using the Brake System

To switch the impedance of the end effector, a simple brake mechanism was also implemented. By engaging the brakes and locking the end effector, DORIS can switch its impedance from the almost zero up to 9000 N/m (Table II), which is stiff enough to be perceived as a virtual wall [10]. Both ends of the five-bar linkage systems connecting the end effector and decoupling mechanism are also connected to solenoid type brakes (112-05-12, Miki Pulley, Kanagawa, Japan) (Fig. 1) through timing

TABLE II
MEASURED MASS, STIFFNESS, AND VISCOSITY PERCEIVED AT THE END EFFECTOR IN THE USER WORKSPACE WHEN THE END EFFECTOR WAS EXCITED (OR THE DECOUPLING MECHANISM WAS EXCITED)

Direction	X	Y
Mass of manipulator (kg)		10
Mass of end effector (kg)	0.20 (0.02)	0.29 (0.02)
Stiffness with brakes released (N/m)	≤ 0.25 (0.18)	≤ 0.25 (0.22)
Stiffness with brakes engaged (N/m)		≥ 9000
Viscosity (N-s/m)	0.90 (1.18)	1.55 (1.36)

belts. A six-axis force and torque (FT) sensor (Mini 45, ATI Industrial Automation, Apex, NC, US) was installed between the decoupling mechanism and the manipulator. After engaging the brakes, imposed contact forces and torques can be readily measured.

C. System Identification

To assess the transparency of the developed robot, DORIS, effective mechanical impedances of the end effector were estimated. Since the 5-bar linkage mechanism, which are connected to the end effector, has different configurations and impedances along the horizontal and vertical directions, each direction of the 2-DOF workspace was modeled separately as a 1-DOF mass-spring-damper system. The effective mass, stiffness, and damping coefficient (viscosity) of the end effector were identified from an estimated transfer function between applied forces on the end effector and the relative movement of the end effector with respect to the decoupling mechanism. Two different but similar tests were conducted to arouse the same magnitude of the relative movement of the end effector within the decoupling mechanism. Firstly, the end effector was excited using another haptic device with the decoupling mechanism controlled motionless. The HapticMaster (Moog Inc., East Aurora, NY, US), which is a programmable haptic robot, excited the end effector at a frequency of 2 Hz, and with an amplitude of 10 mm while measuring interaction forces between the HapticMaster and the end effector of DORIS using a force sensor at the end of the HapticMaster. Secondly, in reverse, the decoupling mechanism was shaken by the developed controller with the end effector remained motionless, and the HapticMaster measured the contact forces. Either way, the same relative movement of the end effector with respect to the decoupling mechanism was produced and offered some resisting forces due to its inertia of the 5-bar linkage systems, and passive revolute joints in the decoupling mechanism (Fig. 1). Notably, the first test could give us the effective impedances imposed on the end effector and user's hand. The second test could assess how much forces were transmitted to the user while the actuators were controlled to follow the user's movements. The impedances from the second test will be some portions of those from the first test.

To determine whether there was any position-dependent non-linearity of the end effector's inertia, a similar test with a different excitation amplitude of 5 mm was conducted. The recorded

contact forces and kinematic data were filtered with the 5th order Butterworth low-pass filter with a cut-off frequency of 3 Hz. Parameters of the impedances were estimated using the MATLAB System Identification Toolbox (MathWorks, Natick, MA, US).

For evaluation of the control performance of DORIS, both a step response and frequency response in reaction to the sinusoidal positional input were recorded. For the frequency response test, the frequency of the positional input signal was swept from 0.1 Hz to 10 Hz with an amplitude of 10 mm. Both the step and sinusoidal position input signals were applied to the controller of DORIS, so that the decoupling mechanism could follow such input movements. Measured positional output was then compared to the positional input signals.

D. Experimental Setup for System Verification

To verify whether DORIS was transparent enough to assess intrinsic voluntary motor control of the human upper limb, kinematic data of seven chronic stroke survivors with hemiparesis (63.84 ± 3.80 years old, 12.75 ± 9.59 years after stroke, and Fugl-Meyer upper extremity motor score of 31.17 ± 14.26 for their affected sides) were collected during target reaching and compared between DORIS and another programmable haptic robot, the HapticMaster. Participants signed informed consent forms (#STU00208823) approved by the Northwestern University Institutional Review Board (IRB) Committee prior to the tests. The upper limbs were supported by the end effector, and subjects were then asked to reach a target (Fig. 7) as fast as possible. The target was 0.2 m apart from the initial position. Subjects repeated the target reaching task seven times. Joint kinematic data and trajectories of the end effector were collected simultaneously using a motion capture system (V120: Trio, OptiTrack, Corvallis, OR, US) and DORIS, respectively. To provide the user with visual feedback of the handle position, a monitor was installed in front of the subjects. A Maximum velocity, maximum acceleration, and jerk of the target reaching movements were calculated to determine which haptic robot was less interfering with the user's voluntary motions.

III. RESULTS

The measured effective mass, stiffness, and damping coefficient of the end effector for either x and y-direction were calculated from the transfer function between the input force measured using the HapticMaster and measured relative position of the end effector of DORIS and are listed in Table II. No matter if the end effector or the decoupling mechanism was excited, the identified elasticity and viscosity imposed on the end effector of DORIS were almost the same (Table II). The inertia, however, was larger with the end effector excited than with the decoupling mechanism excited.

The 1-DOF model with estimated parameters successfully reproduced the positional output with the measured sinusoidal input forces from the HapticMaster and showed an error of 4% as compared to the measured positional output. Since the end effector was connected to the decoupling mechanism through the

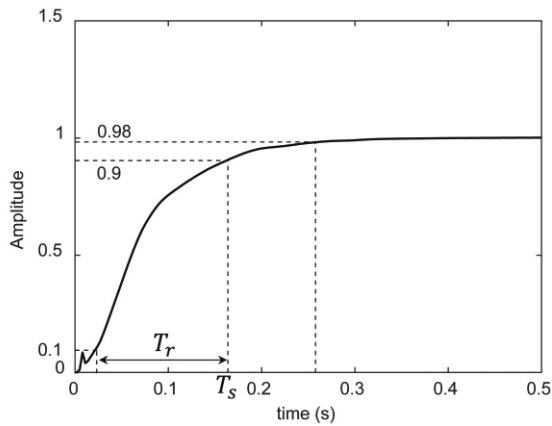


Fig. 5. Step response (position) of the decoupling mechanism of DORIS with a step positional input to the controller. A rise time (T_r) and settling time (T_s) were found as 0.138 and 0.252 s, respectively.

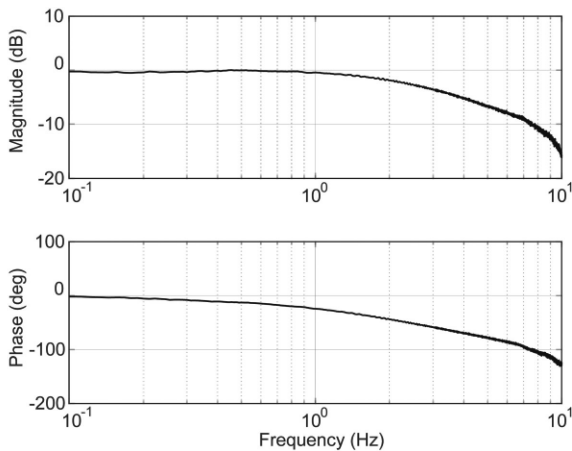


Fig. 6. Frequency response for identification of the system parameters and control bandwidth of the closed-loop controller employed in the robot. In response to the given positional input signal at frequencies swept from 0.1 to 10 Hz, the amplitude of the output (position of the decoupling mechanism) reduced to half at a frequency of 2.6 Hz.

5-bar linkage system, effective impedances could vary with different positions of the end effector and correspondingly different configurations of the 5-bar linkage. With a different amplitude of 5 mm while being excited, the effective mass of the end effector increased by 4.9%.

Given a unit positional step input to the controller of DORIS, the rise time and settling time were found to be 0.138 s and 0.252 s, respectively (Fig. 5). When excited by the HapticMaster with frequencies swept from 0.1 to 10 Hz, the frequency response of the end effector is presented in Fig. 6. As the frequency of positional input increased, the amplitude of the output position tended to decrease. From the frequency response plot, the amplitude of the measured gain of the end effector decreased by half at frequencies higher than 2.6 Hz, which determined the control bandwidth of the developed DORIS as 2.6 Hz.

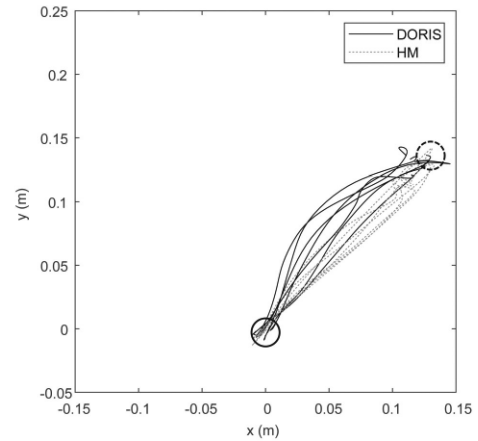


Fig. 7. Reaching trajectories from a representative subject with right hemiparesis with DORIS (black solid lines) and the HapticMaster (HM, gray dashed lines). Starting from a home target (solid circle), subjects reached the right target (dashed circle). Please note that stroke survivors with left hemiparesis reached the left target.

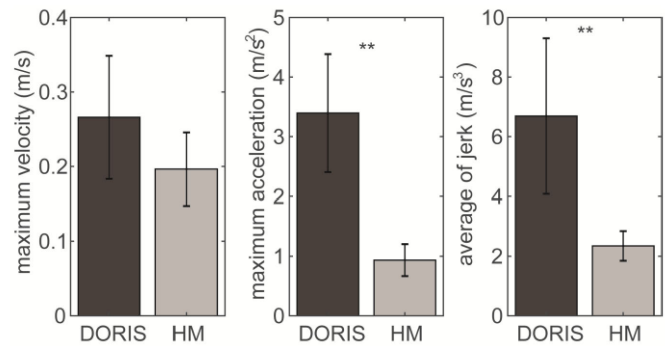


Fig. 8. Comparison of a maximum velocity (left), maximum acceleration (middle), and average of jerk (right) of the reaching movement between DORIS (black) and the HapticMaster (HM, gray) with 1 SD. ** $p < .01$.

All participants successfully completed the target reaching task while their affected sides of the upper limb were being supported by DORIS. Representative trajectories with DORIS and the HapticMaster are shown in Fig. 7. Measured friction and elastic forces counteracting movements were maintained below 0.09 N and 0.19 N at the maximum displacement and measured speed of the end effector (Table I), respectively. An average of maximum velocity, maximum acceleration, and average of jerk for the target reaching were 0.20 ± 0.05 m/s, 0.93 ± 0.27 m/s², and 2.34 ± 0.50 m/s³ with the HapticMaster and were 0.27 ± 0.08 m/s, 3.40 ± 1.00 m/s², and 6.69 ± 2.61 m/s³ with DORIS, respectively (Fig. 8).

IV. DISCUSSION

In this study, we describe the design and performance of a new planar haptic robot, called DORIS. It was designed to provide a user with minimum undesired impedances, with the idea that it can be used to explore rigorously the interaction between limb trajectory control and complex external impedance loads.

DORIS was also utilized to assess jerky movements of the upper limb for target reaching task in chronic stroke survivors with hemiparesis. Our results imply that the device can be used for assessment of intrinsic voluntary motor control of the upper limb. Additional advantages, which are derived from the proposed decoupling mechanism, and applications of DORIS with minimized impedances are further described hereafter.

A. Reduced Impedance of the Robot and Its Effects on Voluntary Arm Movements

Although many different haptic devices [3], [8], [9], [13], [15]–[19], [21], [22] have been developed and widely utilized to assess voluntary motor control of the upper limb, limited transparency of the end effector often affects the voluntary movement. As reported previously, mildly impaired chronic stroke survivors showed larger joint excursions and smoother velocity profiles in a 2-D reaching task when their upper limbs were supported against gravity [1], [34]–[37] and when friction forces were sharply reduced [1]. This result implies that reduced loading on upper limb and minimized mechanical impedances could reveal the preservation of motor control of upper limbs in patients with neurological disorders.

Since then, several published studies [35]–[37] have been conducted to explore undesired activation patterns or weakness in upper limb muscles of stroke survivors using haptic devices or manipulators. Such devices, however, impose a non-negligible, additional inertia of up to 2 kg [10], [16] on the subject's arm, which has a similar magnitude of mass of the normal upper limb [38]. The device may also add additional viscosity [39]. Since additional inertial or viscous loads imposed by manipulators could disturb the kinematics of the upper limb and change the activation level of the upper limb [2], such additional loads imposed by haptic devices should ideally be minimized.

To minimize additional loads imposed by haptic devices, several mechanical systems or control paradigms have been suggested. Beer and his colleagues [1] used an air-bearing to minimize friction forces. Badesa and his colleagues [40] developed a planar robot driven by pneumatic swivel modules. Gomi and Kawato developed a 2-D planar haptic robot that consists of links and an air-magnetic floating mechanism to avoid friction. The user, however, still have to manipulate an additional inertia of 2 kg [16] or an additional viscosity of 4.40 N-s/m [39]. Other well-known back-drivable haptic devices include the MIT MANUS and the KINARM. Each has multiple linkage systems that exhibit a relatively large effective mass of 0.67 kg [10] and a total mass of the linkage systems of 1.348 kg [3], [20], respectively. Another haptic device, the MEDARM, utilizing cable systems to transmit actuating torques and to reduce its inertia shows almost twice as large as the KINARM on the shoulder joint [3].

A larger workspace required for the assessment of upper limb control could also introduce a larger inertial load. When developing a robotic manipulator, a limitation in minimizing the inertia of the manipulator comes from the fact that longer

linkages being used for the manipulator are necessarily accompanied by increased inertia. Since the inertia of the manipulator is proportional to the mass and square of the length of the links, shorter links are preferable to decrease inertia of the manipulator. However, since shorter links limit the workspace of the user, a unique mechanism that decouples a long linkage system and actuators from the user's workspace is deemed necessary, and such a system is proposed here in this study.

Here, the end effector of DORIS is decoupled from the actuators and linkage system, so the most of mechanical impedances imposed by the manipulator could also be isolated from the user. Though the mass of the manipulator including the linkage systems and decoupling mechanism is larger than 10 kg, both the decoupled end effector and a user are largely unaffected by these additional inertial load. For example, when exciting the decoupling mechanism with the end effector in a fixed position, actuating forces exerted on the decoupling mechanism were larger than 20 N, but the measured contact forces between the end effector and HapticMaster remained below 0.19 N, which implies that the most of actuating forces were not transmitted to the end effector. As compared to conventional haptic robots, the new haptic robot can reduce its effective mass to a one-sixth or one half (Table II) of the minimum effective mass of a different, widely used robotic manipulator, the HapticMaster (2 kg) [16] or of the MIT MANUS (2/3 kg) [10], respectively. Furthermore, a viscosity perceived at the end effector was reduced to nearly one-third when compared to a previously developed haptic manipulator [39]. Interestingly, link-driven haptic robots have position-dependent impedances of the end effector due to different link configurations and correspondingly different moment of inertias in a large workspace. Our robot, however, imposes impedances which are induced by relative movements of the end effector in the small (user) workspace, so mechanical impedances are similar across the large (manipulator) workspace. It is worth reporting the measured impedances of the end effector represent its minimum values. Since the weight of the user's upper limbs can add additional loading vertically on the end effector and surrounding components, the impedances perceived at the end effector may vary slightly. Though this was not tested, the deformation due to the vertical loading and resultant increase in friction forces would be expected to be negligible.

The developed robot, DORIS, is sensitive to user's manipulating forces so is also capable of detecting a larger magnitude of acceleration and larger jerk during the target reaching task in stroke survivors. As compared to the HapticMaster, the effective inertia decreased by approximately one-sixth so resulting acceleration increased by more than three times (Fig. 8). This result implies that an additional mass of 2 kg on the upper limb, in contrast, could scale the maximum acceleration down by half with the same joint torques. Another important parameter describing how smoothly the users control their voluntary movements is jerk, which is defined as a rate of change of movement acceleration [41]. The more transparent and sensitive the new robot was to users' manipulating forces, the jerkier reaching movements became. Both the maximum acceleration and jerk were significantly larger with DORIS compared to the HapticMaster, which

implies that undesired, additional impedances of the end effector may disturb user's intrinsic control performance and shade any types of jerky movements of the upper limb.

B. Bandwidth of Control System

The bandwidth of the control system employed in our new robot is also higher than the maximum frequency content of the type I movement of hands and fingers (2 Hz), which is defined as a range of voluntary movements conducted without a decrease in amplitude as compared to the magnitude of intended motions and can also be tracked by eyes. The available control bandwidth, however, is lower than the maximum frequency content of rapid movements of hands and fingers (8 Hz) [42]. This is one of the limitations of our robot.

Since our target reaching tasks relied on visual feedback, which is a type I movements (≤ 2 Hz) and do not utilize maximum voluntary movement speed (type II), no subject hit the boundary of the decoupling mechanism. If subjects move faster than the maximum speed of the decoupling mechanism (1.7 m/s) at a higher frequency than the control bandwidth (2.6 Hz), they can possibly, in principle, bottom out the boundary of the decoupling mechanism. This would then engage the inertia of the whole manipulator, which potentially weighs over 10 kg, and actuating forces transmitted by the robot arms on the end effector. Although such fast movement is not the intended operating situation for DORIS, it is one of its potential limitations.

C. Switchable Impedance of DORIS Using the Brake System and FT Sensor

Inspired by positive results from several published studies, which suggested that interacting with virtual haptic objects could both help users focus more on the task [34] and induce a high level of cortical activity [33], a simply switchable impedance of the end effector was achieved by engaging the brake system. As the brake system holds the end effector, its movement can be restrained, and the stiffness can be switched from 0.25 to 9000 N/m (Table II). Notably, only when the end effector is being held by the brake system, the FT sensor, which is connected to the decoupling mechanism, can measure manipulating forces exerted by the user. Though only the switchable impedance has been enabled for DORIS so far, measured manipulating forces, for example, can be further utilized to simulate variable impedance such as viscous or elastic load, based on a pre-defined relationship between the manipulating forces and kinematics of the manipulator, which was already well developed by the admittance control paradigm [16].

V. CONCLUSION

We have developed and tested a new robotic haptic manipulator called DORIS, which exhibits substantially reduced impedances of the end effector. Since the decoupling mechanism of the manipulator was designed to track user's input movements but not to transmit the impedances of all the linkage systems and actuators to the end effector, the effective impedance perceived at the end effector by a user could be substantially reduced, no

matter what size of workspace was employed. When compared to another advanced and widely used programmable haptic robot, DORIS was more sensitive to user's manipulating forces so was also capable of detecting undisturbed movements of the upper limb in stroke survivors.

Since motor control of the upper limb of stroke survivors has been found to be very sensitive to loading conditions, our new manipulator can potentially be utilized to examine the preservation of the motor control with minimal loading on subjects' muscles.

REFERENCES

- [1] R. F. Beer *et al.*, "Target-dependent differences between free and constrained arm movements in chronic hemiparesis," *Exp. Brain Res.*, vol. 156, pp. 458–470, 2004.
- [2] T. M. Stoeckmann, K. J. Sullivan, and R. A. Scheidt, "Elastic, viscous, and mass load effects on poststroke muscle recruitment and co-contraction during reaching: A pilot study," *Phys. Ther.*, vol. 89, pp. 665–678, 2009.
- [3] S. J. Ball, I. E. Brown, and S. H. Scott, "Performance evaluation of a planar 3DOF robotic exoskeleton for motor assessment," *J. Med. Devices*, vol. 3, no. 2, 2009.
- [4] S. Fahmi and T. Hulin, "Inertial properties in haptic devices: Non-linear inertia shaping vs. force feedforward," *IFAC-PapersOnLine*, vol. 51, no. 22, pp. 79–84, 2018.
- [5] M. Casadio *et al.*, "Functional reorganization of upper-body movement after spinal cord injury," *Exp. Brain Res.*, vol. 207, no. 3–4, pp. 233–247, 2010.
- [6] L. Dipietro *et al.*, "Submovement changes characterize generalization of motor recovery after stroke," *Cortex*, vol. 45, no. 3, pp. 318–324, 2009.
- [7] S. Hesse, H. Schmidt, and C. Werner, "Machines to support motor rehabilitation after stroke: 10 years of experience in Berlin," *J. Rehabil. Res. Develop.*, vol. 43, no. 5, pp. 671–678, 2006.
- [8] S.-W. Pu and J.-Y. Chang, "Robotic hand system design for mirror therapy rehabilitation after stroke," *Microsyst. Technol.*, vol. 26, no. 1, pp. 111–119, 2019.
- [9] N. Hogan *et al.*, "MIT-MANUS: A workstation for manual therapy and training. I," *Proc. IEEE Int. Workshop Robot Hum. Commun.*, Tokyo, Japan, 1992, pp. 161–165, doi: [10.1109/ROMAN.1992.253895](https://doi.org/10.1109/ROMAN.1992.253895).
- [10] H. I. Krebs *et al.*, "Rehabilitation robotics: Pilot trial of a spatial extension for MIT-Manus," *J. Neuroeng. Rehabil.*, vol. 1, pp. 1–15, 2004.
- [11] Y.-W. Hsieh *et al.*, "Comparison of proximal versus distal upper-limb robotic rehabilitation on motor performance after stroke: A cluster controlled trial," *Sci. Rep.*, vol. 8, no. 1, pp. 1–11, 2018.
- [12] S. Mazzoleni *et al.*, "Wrist robot-assisted rehabilitation treatment in subacute and chronic stroke patients: From distal-to-proximal motor recovery," *IEEE Trans. Neural Syst. Rehabil. Eng.*, vol. 26, no. 9, pp. 1889–1896, Sep. 2018.
- [13] B. E. Perry, E. K. Evans, and D. S. Stokic, "Weight compensation characteristics of armo spring exoskeleton: Implications for clinical practice and research," *J. Neuroeng. Rehabil.*, vol. 14, no. 1, pp. 1–10, 2017.
- [14] F. Just *et al.*, "Online adaptive compensation of the ARMin rehabilitation robot," *Biomechatronics (BioRob)*, Singapore, 2016, pp. 747–752, doi: [10.1109/BIOROB.2016.7523716](https://doi.org/10.1109/BIOROB.2016.7523716).
- [15] C. Adans-Dester *et al.*, "Upper extremity rehabilitation with the BURT robotic arm," *Arch. Phys. Med. Rehabil.*, vol. 100, no. 12, pp. e208–e209, 2019.
- [16] R. Q. Van Der Linde and P. Lammertse, "HapticMaster - A generic force controlled robot for human interaction," *Ind. Robot*, vol. 30, pp. 515–524, 2003.
- [17] R. V. D. Linde *et al.*, "The hapticmaster, a new high-performance haptic interface," in *Proc. EuroHaptic*, Edinburgh, U.K., 2002, pp. 1–5.
- [18] E. de Vlugt *et al.*, "A force-controlled planar haptic device for movement control analysis of the human arm," *J. Neurosci. Methods*, vol. 129, no. 2, pp. 151–168, 2003.
- [19] J. C. Fraile *et al.*, "E2Rebot: A robotic platform for upper limb rehabilitation in patients with neuromotor disability," *Adv. Mech. Eng.*, vol. 8, no. 8, 2016, Art. no. 1687814016659050.
- [20] S. H. Scott, "Apparatus for measuring and perturbing shoulder and elbow joint positions and torques during reaching," *J. Neurosci. Methods*, vol. 89, no. 2, pp. 119–127, 1999.

- [21] G. Boschetti and A. Trevisani, "Cable robot performance evaluation by wrench exertion capability," *Robotics*, vol. 7, no. 2, p. 15, 2018.
- [22] I. S. Howard, J. N. Ingram, and D. M. Wolpert, "A modular planar robotic manipulandum with end-point torque control," *J. Neurosci. Methods*, vol. 181, no. 2, pp. 199–211, Jul. 30, 2009.
- [23] L. Zollo *et al.*, "Dynamic characterization and interaction control of the CBM-Motus robot for upper-limb rehabilitation," *Int. J. Adv. Robotic Syst.*, vol. 10, no. 10, 2013, Art. no. 374.
- [24] N. Karbasizadeh *et al.*, "Experimental dynamic identification and model feed-forward control of Novint falcon haptic device," *Mechatronics*, vol. 51, pp. 19–30, 2018.
- [25] A. Q. Keemink, H. van der Kooij, and A. H. Stienen, "Admittance control for physical human–robot interaction," *Int. J. Robot. Res.*, vol. 37, no. 11, pp. 1421–1444, 2018.
- [26] K. H. Lee *et al.*, "Enhanced transparency for physical human-robot interaction using human hand impedance compensation," *IEEE/ASME Trans. Mechatronics*, vol. 23, no. 6, pp. 2662–2670, Dec. 2018.
- [27] X. Chen *et al.*, "Neural learning enhanced variable admittance control for human–robot collaboration," *IEEE Access*, vol. 8, pp. 25727–25737, 2020.
- [28] C. T. Freeman, "Upper limb electrical stimulation using input-output linearization and iterative learning control," *IEEE Trans. Control Syst. Technol.*, vol. 23, no. 4, pp. 1546–1554, Jul. 2015.
- [29] C. Yang *et al.*, "Human-like adaptation of force and impedance in stable and unstable interactions," *IEEE Trans. Robot.*, vol. 27, no. 5, pp. 918–930, Oct. 2011.
- [30] P. D. Labrecque, J.-M. Haché, M. Abdallah, and C. Gosselin, "Low-impedance physical human-robot interaction using an active–passive dynamics decoupling," *IEEE Robot. Automat. Lett.*, vol. 1, no. 2, pp. 938–945, Jul. 2016.
- [31] R. Chu *et al.*, "Co-actuation: A method for achieving high stiffness and low inertia for haptic devices," *IEEE Trans. Haptics*, vol. 13, no. 2, pp. 312–324, Apr.-Jun. 2020.
- [32] M. Cui, Z. Zhang, and P. Yan, "Tracking control of a large range 3D printed compliant nano-manipulator with enhanced anti-windup compensation," *Mech. Syst. Signal Process.*, vol. 131, pp. 33–48, 2019.
- [33] A. Merians *et al.*, "Innovative approaches to the rehabilitation of upper extremity hemiparesis using virtual environments," *Eur. J. Phys. Rehabil. Med.*, vol. 45, no. 1, pp. 123–133, 2009.
- [34] G. B. Prange *et al.*, "The effect of arm support combined with rehabilitation games on upper-extremity function in subacute stroke: A randomized controlled trial," *Neurorehabil. Neural Repair*, vol. 29, pp. 174–182, 2015.
- [35] M. D. Ellis, I. Schut, and J. P. A. Dewald, "Flexion synergy overshadows flexor spasticity during reaching in chronic moderate to severe hemiparetic stroke," *Clin. Neurophysiol.*, vol. 128, pp. 1308–1314, 2017.
- [36] T. M. Sukal, M. D. Ellis, and J. P. A. Dewald, "Shoulder abduction-induced reductions in reaching work area following hemiparetic stroke: Neuroscientific implications," *Exp. Brain Res.*, vol. 183, pp. 215–223, 2007.
- [37] R. F. Beer *et al.*, "Impact of gravity loading on post-stroke reaching and its relationship to weakness," *Muscle Nerve*, vol. 36, pp. 242–250, 2007.
- [38] M. J. Pavol, T. M. Owings, and M. D. Grabiner, "Body segment inertial parameter estimation for the general population of older adults," *J. Biomech.*, vol. 35, no. 5, pp. 707–712, 2002.
- [39] H. Gomi and M. Kawato, "Human arm stiffness and equilibrium-point trajectory during multi-joint movement," *Biol. Cybern.*, vol. 76, pp. 163–171, 1997.
- [40] F. J. Badesa *et al.*, "Pneumatic planar rehabilitation robot for post-stroke patients," *Biomed. Eng.: Appl., Basis Commun.*, vol. 26, pp. 1450025, 2014.
- [41] T. Flash and N. Hogan, "The coordination of arm movements: An experimentally confirmed mathematical model," *J. Neurosci.*, vol. 5, no. 7, pp. 1688–1703, 1985.
- [42] H.-J. Freund, "Time control of hand movements," in *Progress in Brain Research*. Amsterdam, The Netherlands: Elsevier, 1986, pp. 287–294.